Supporting Information for

Effect of the Electric Double Layer (EDL) in Multicomponent Electrolyte Reduction and Solid Electrolyte Interphase (SEI) Formation in Lithium Batteries

Qisheng Wu[1], Matthew T. McDowell[2], and Yue Qi[1,*]

[1]School of Engineering, Brown University, Providence, RI 02912, United States

[2]G. W. Woodruff School of Mechanical Engineering and School of Materials Science and Engineering, Georgia Institute of Technology, Atlanta, GA 30332, United States

*Corresponding author: Y. Q. (yueqi@brown.edu)

Molecular Dynamics simulation details

All MD simulations used the COMPASS III force field with force type and charges shown in Part I.

The MD simulations of bulk electrolytes (Part II) were first conducted under the constant particle number, volume, and temperature (NPT) ensemble for 1.0 ns at room temperature (20 ℃), followed by another 1.0 ns equilibration run under NPT ensemble at target temperatures, which are set to only room temperature (20 ℃) for the carbonate-based electrolytes but both room and low temperatures (20 ℃ and -40 ℃) for the ether-based electrolytes. Then production runs under the NPT ensemble were conducted for 4.0 ns for statistical analyses to obtain the Li-ion conductivity and Li-ion solvation shell (reported in Part II). The average density and coordination number (CN) are converged within 1.0 ns.

For MD simulations of EDL (Part III), pre-equilibration runs were first conducted for 0.2 ns under NVT ensemble at the target temperatures to obtain the equilibrated distance between the two graphene electrodes under uncharged conditions, during which the graphene electrodes were allowed to move along the direction perpendicular to graphene plane. The graphene electrodes were then fixed for the subsequent simulations. The interfacial systems were equilibrated for 2.0 ns at 20 ℃ under NVT ensemble under uncharged conditions and then for 4.0 ns at the target temperatures (again only 20 ℃ for the carbonate-based electrolytes but both 20 ℃ and -40 ℃ for the ether-based electrolytes) under each charge density

condition. The number of different specites in the DEL concerged in 3.0 ns. Adding another 4.0 ns will not further change any average values by 10%.

Part I, Force field calibration

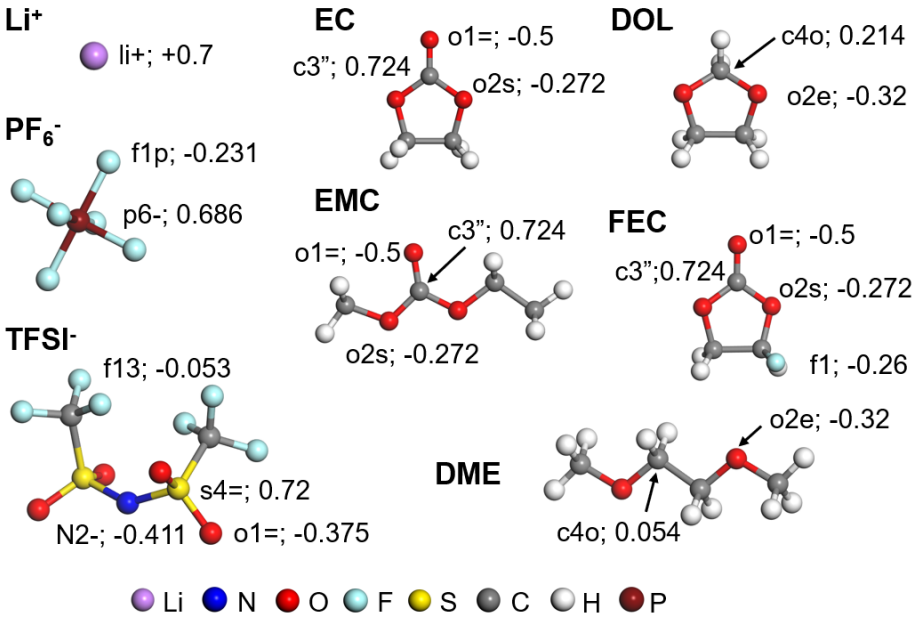

Figure S1. Electrolyte species investigated in this work, including $LiPF_6$, EC, EMC, FEC, LiTFSI, DOL and DME. Representative atom types and atomic charges are given accordingly. Purple, blue, red, light blue, yellow, grey, white, and brown spheres represent Li, N, O, F, S, C, H, and P atoms, respectively.

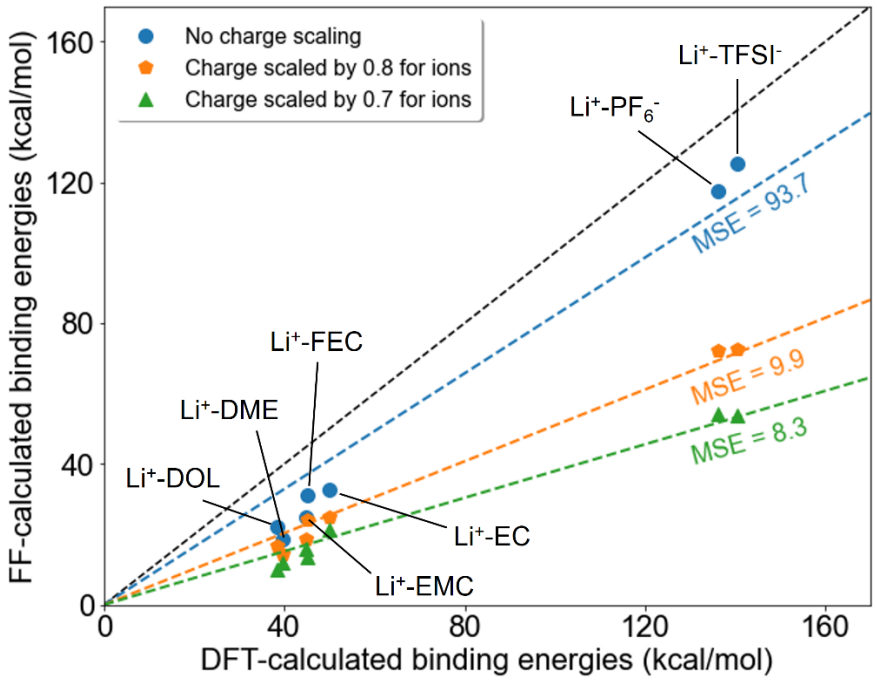

Figure S2. Binding energies calculated based on COMPASS III force field (FF) as functions of binding energies calculated based on DFT method (see main text for details of both FF- and DFT-based calculations). Blue dots refer to the FF-calculated binding energies without charge scales, while orange and green dots refer to the binding energies calculated based on charge scales of 0.8 and 0.7, respectively. The blue, orange, and green dash lines are corresponding linear fittings with intercept of zero. It is seen that the mean squared errors (MSE, in kcal/mol) of the linear fittings are largely reduced with charge scales of 0.8 and 0.7, which indicate the cation-anion and cation-solvent interactions become more balanced. The scale of 0.7 is used in this work for all the MD simulations, with which the calculated densities and Li^+ conductivities for the both carbonate-based and ether-based electrolytes agree well with experimentally measured data (See **Figure S3** and **S5** for detailed comparisons).

Part II, Bulk Electrolytes

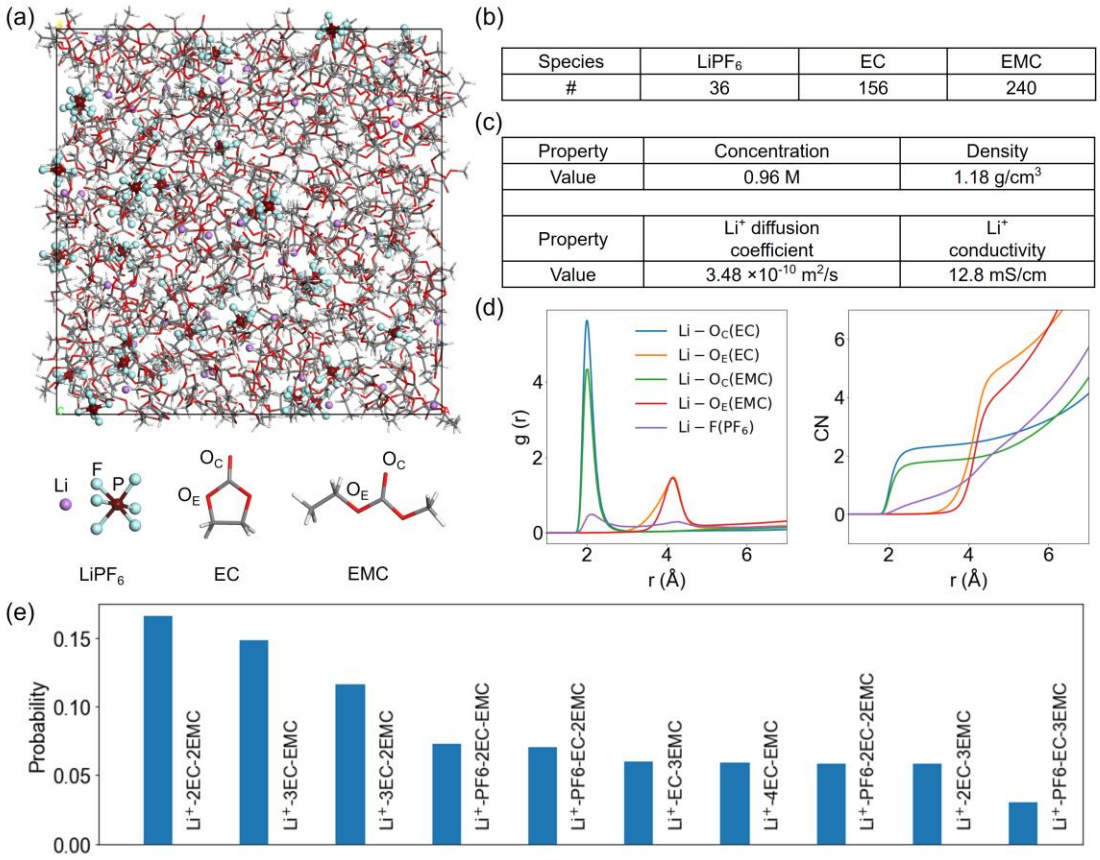

Species	$LiPF_6$	EC	EMC
#	36	156	240

Property	Concentration	Density
Value	0.96 M	1.18 g/cm^3
Property	Li^+ diffusion coefficient	Li^+ conductivity
Value	3.48 ×10^{-10} m^2/s	12.8 mS/cm

Figure S3. MD simulations of the bulk electrolyte containing $LiPF_6$ salt in the mixed EC/EMC electrolyte ($LiPF_6$@EC:EMC). The molar ratio of $LiPF_6$:EC:EMC is set to 3:13:20 to mimic the molar concentration of ~1.0 M and the volume ratio of EC:EMC=3:7 that was used in the experiment.[1] (a) An MD snapshot at 20 °C. (b) Table list of the number of species in the simulation system, including 36 $LiPF_6$, 156 EC and 240 EMC. (c) Table list of MD-calculated properties (concentration, density, diffusion coefficient and conductivity) of the simulated bulk electrolyte. Both calculated density and Li^+ conductivity agree well with previous experimental and theoretical values.[2,3] (d) Calculated averaged Li^+ to PF_6^-/EC/EMC coordination numbers as well as total coordination number. Following our previous work,[4] radial distribution functions are referenced to total number density of O and F atoms. (e) Radial distribution function *g(r)* (RDF, left panel) and coordination number (CN, right panel) plots of Li^+ ions to F and O atoms as functions of atom distances. O_C and O_E represent carbonyl oxygen and ester oxygen, respectively, in EC and EMC molecules. (f) Probability distributions of the solvation structures of the first solvation shell of Li^+ ions in the $LiPF_6$@EC:EMC electrolyte. For example, "2EC-2EMC" refers to that Li^+ is coordinated with 2 EC and 2 EMC molecules. Only ten solvation shell structures with the highest probabilities are shown.

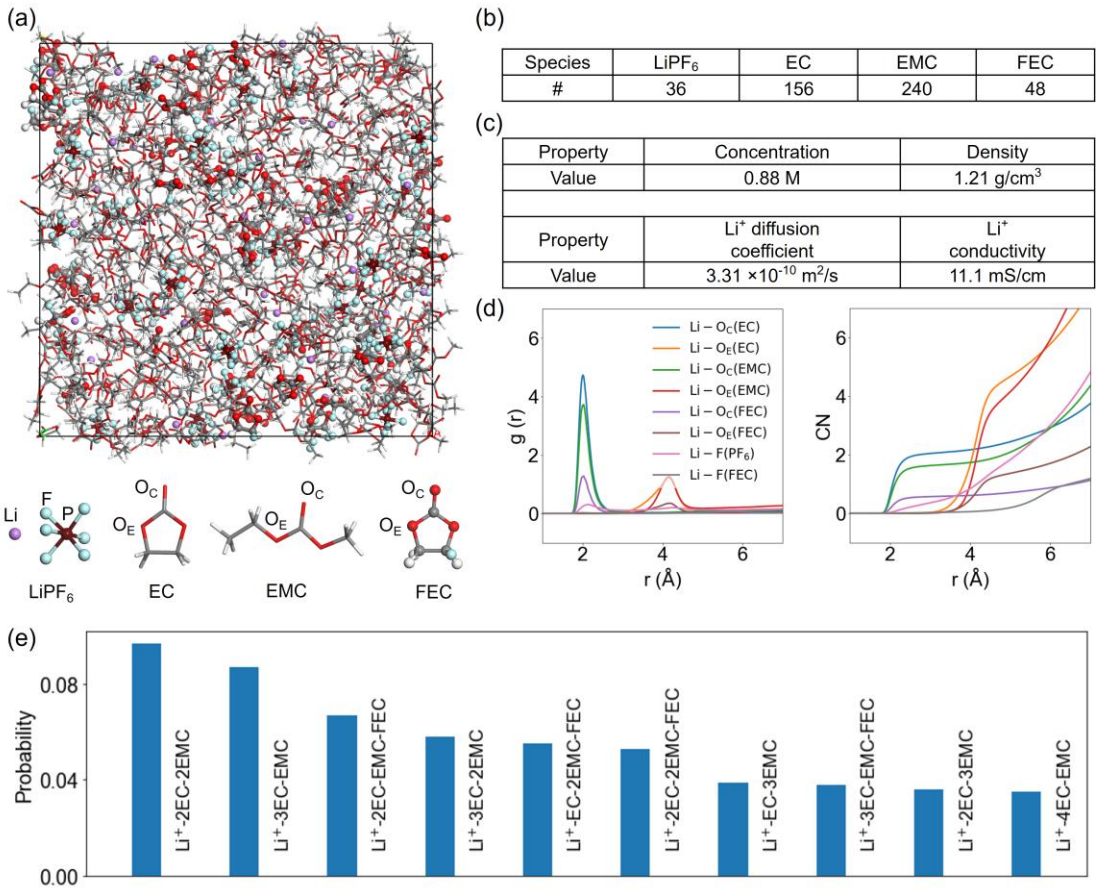

Species	$LiPF_6$	EC	EMC	FEC
#	36	156	240	48

Property	Concentration	Density
Value	0.88 M	1.21 g/cm^3

Property	Li^+ diffusion coefficient	Li^+ conductivity
Value	3.31 ×10^{-10} m^2/s	11.1 mS/cm

Figure S4. MD simulations of bulk $LiPF_6$@EC:EMC:FEC. The molar ratio is set to $LiPF_6$:EC:EMC:FEC=3:13:20:4. The $LiPF_6$@EC:EMC:FEC electrolyte shows a volume increase of 8.9% compared to $LiPF_6$@EC:EMC after adding FEC. (a) MD snapshot at 20 °C. (b) Table list of the number of species in the simulation system, including 36 $LiPF_6$, 156 EC, 240 EMC and 48 FEC. (c) Table list of MD-calculated properties of the simulated bulk electrolyte. (d) Calculated averaged Li^+ to PF_6^-/EC/EMC coordination numbers as well as total coordination number. Radial distribution functions are referenced to total number density of O and F atoms. (e) Radial distribution function *g(r)* (RDF, left panel) and coordination number (CN, right panel) plots of Li^+ ions to F and O atoms against distance. O_C and O_E represent carbonyl oxygen and ester oxygen, respectively, in EC, EMC and FEC molecules. (f) Probability distributions of the solvation structures of the first solvation shell of Li^+ ions in the $LiPF_6$@EC:EMC:FEC electrolyte. Only ten solvation shell structures with the highest probabilities are shown.

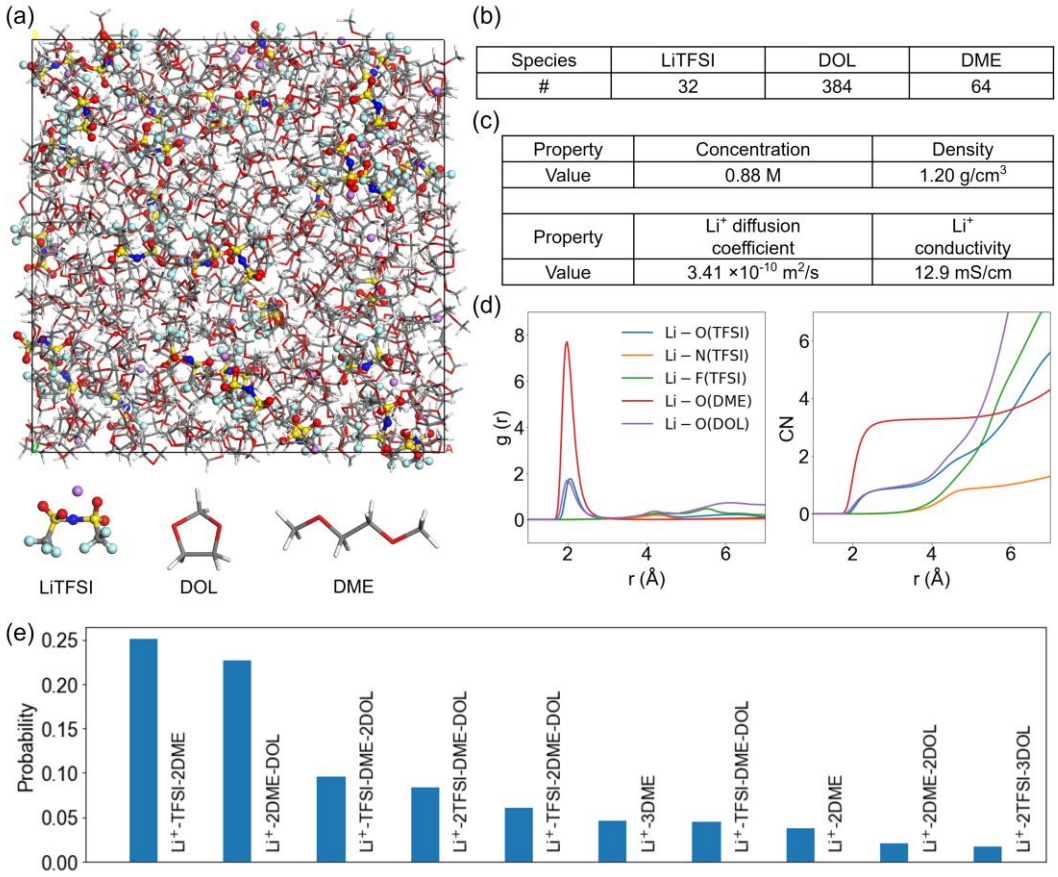

Species	LiTFSI	DOL	DME
#	32	384	64

Property	Concentration	Density
Value	0.88 M	1.20 g/cm^3

Property	Li^+ diffusion coefficient	Li^+ conductivity
Value	3.41 ×10^{-10} m^2/s	12.9 mS/cm

Figure S5. MD simulations of bulk LiTFSI@DOL:DME (~0.9 M). (a) MD snapshot at 20 °C. (b) Table list of the number of species in the simulation system, including 32 LiTFSI, 384 DOL and 64 DME molecules. The molar ratio is set to LiTFSI:DOL:DME=1:12:2 to be consistent with the previous report.[4] (c) Table list of MD-calculated properties of the simulated bulk electrolyte. The calculated Li^+ conductivity agrees well with the previous experimental value.[5] (d) Calculated averaged Li^+ to PF_6^-/EC/EMC coordination numbers as well as total coordination number. Radial distribution functions are referenced to total number density of O, F and N atoms. (e) Radial distribution function *g(r)* (RDF, left panel) and coordination number (CN, right panel) plots of Li^+ ions to F and O atoms against distance. (f) Probability distributions of the solvation structures of the first solvation shell of Li^+ ions in the LiTFSI@DOL:DME electrolyte. Only ten solvation shell structures with the highest probabilities are shown.

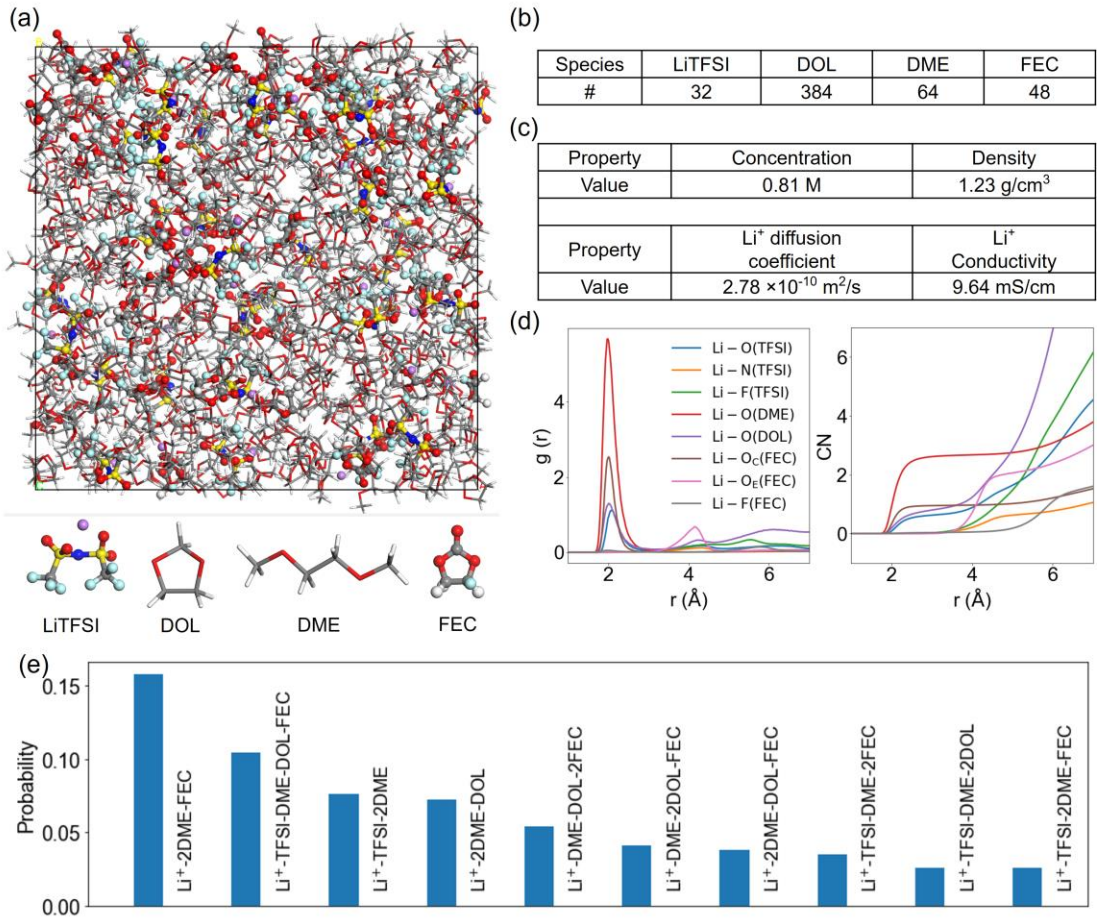

Species	LiTFSI	DOL	DME	FEC
#	32	384	64	48

Property	Concentration	Density
Value	0.81 M	1.23 g/cm^3

Property	Li$^+$ diffusion coefficient	Li$^+$ Conductivity
Value	2.78 ×10^{-10} m^2/s	9.64 mS/cm

Figure S6. MD simulations of bulk LiTFSI@DOL:DME:FEC. (a) MD snapshot at 20 °C. (b) Table list of the number of species in the simulation system, including 32 LiTFSI, 384 DOL, 64 DME and 48 FEC molecules. The molar ratio is set to LiTFSI@DOL:DME:FEC=1:12:2:1.5 to be consistent with the previous report.[4] The LiTFSI@DOL:DME:FEC electrolyte shows a volume increase of 9.2% compared to LiTFSI@DOL:DME after adding FEC. (c) Table list of MD-calculated properties of the simulated bulk electrolyte. (d) Calculated averaged Li^+ to PF_6^- /EC/EMC coordination numbers as well as total coordination number. Radial distribution functions are referenced to total number density of O, F and N atoms. (e) Radial distribution function *g(r)* (RDF, left panel) and coordination number (CN, right panel) plots of Li^+ ions to F and O atoms against distance. O_C and O_E represent carbonyl oxygen and ester oxygen, respectively, in FEC molecule. (f) Probability distributions of the solvation structures of the first solvation shell of Li^+ ions in LiTFSI@DOL:DME:FEC. Only ten solvation shell structures with the highest probabilities are shown.

Part III, EDL structures of carbonate-based electrolytes

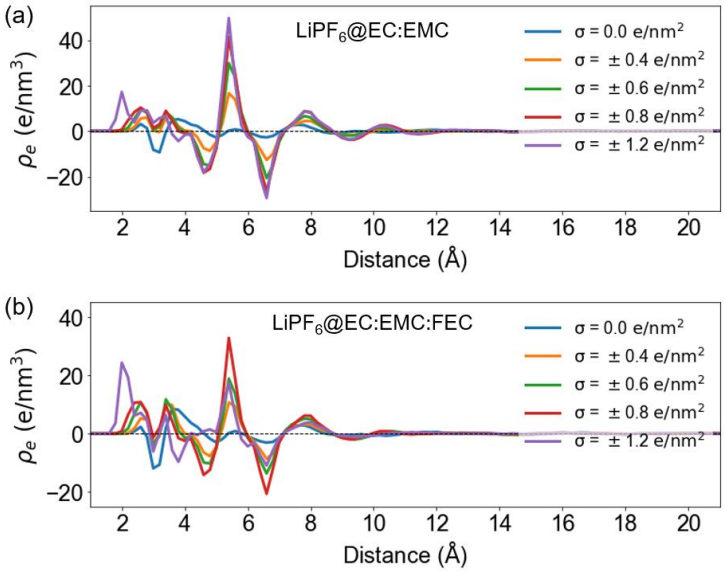

Figure S7. Charge density profiles as functions of distances from the negatively charged graphene electrode for the (a) $LiPF_6$@EC:EMC and (b) $LiPF_6$@EC:EMC:FEC electrolytes under different charging conditions.

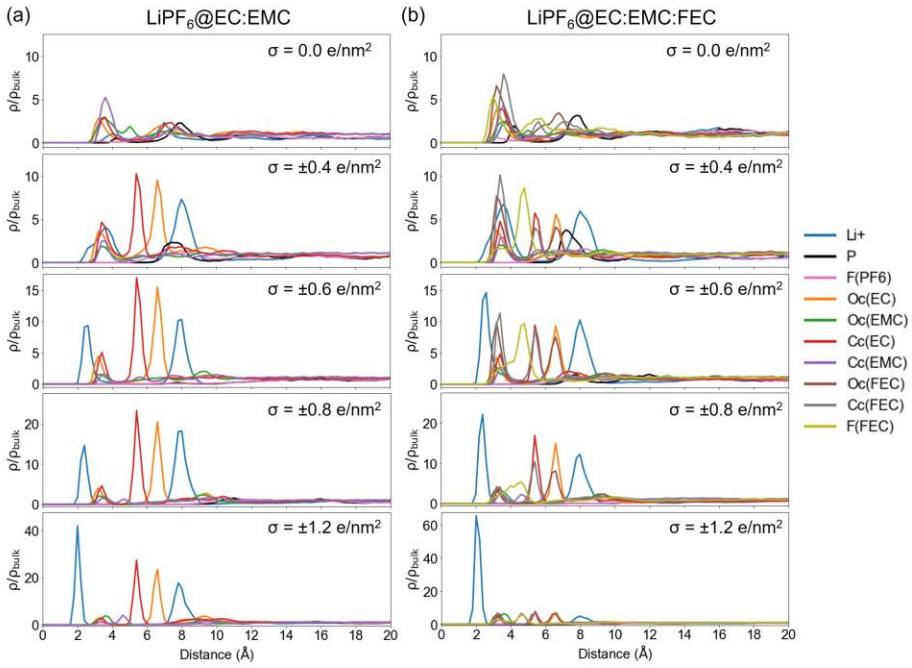

Figure S8. Normalized number density profiles for Li^+ ions and the atoms of interest in EC, EMC, and FEC molecules for the (a) $LiPF_6$@EC:EMC and (b) $LiPF_6$@EC:EMC:FEC electrolytes under different charging conditions.

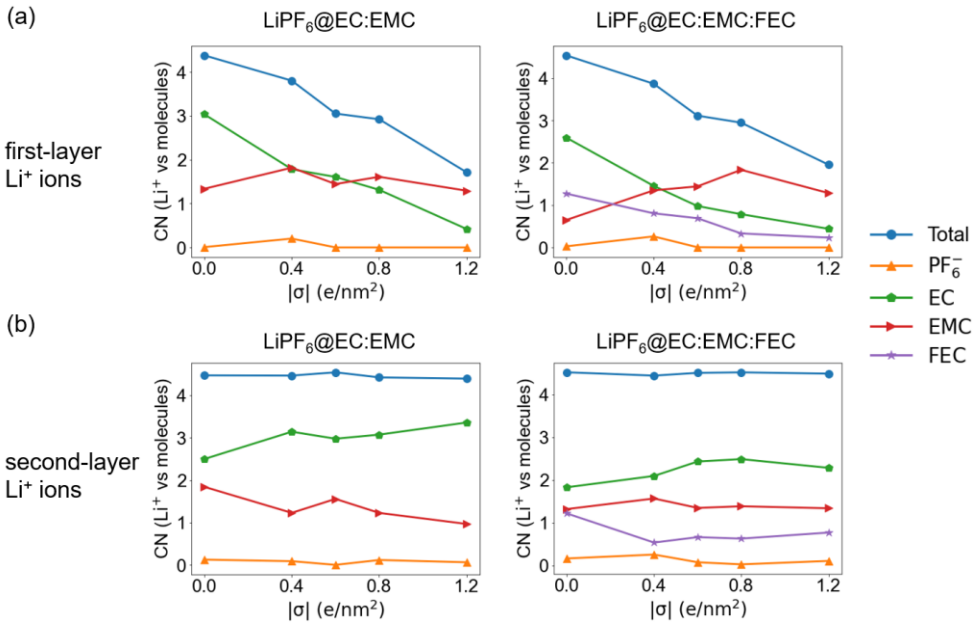

Figure S9. (a) Coordination numbers between the first-layer Li^+ ions (<5.0 Å within the negatively charged graphene electrode) and molecular species (PF_6^-, EC, EMC and FEC) of the EDL as functions of graphene electrode charge densities for $LiPF_6$@EC:EMC (left panel) and $LiPF_6$@EC:EMC:FEC (right panel) electrolytes. (b) Coordination numbers between the second-layer Li^+ ions (5.0-10.0 Å within the negatively charged graphene electrode) and molecular species (PF_6^-, EC, EMC and FEC) of the EDL as functions of graphene electrode charge densities for $LiPF_6$@EC:EMC (left panel) and $LiPF_6$@EC:EMC:FEC (right panel) electrolytes.

Part IV, Reduction potentials of EDL structures for the carbonate-based electrolytes

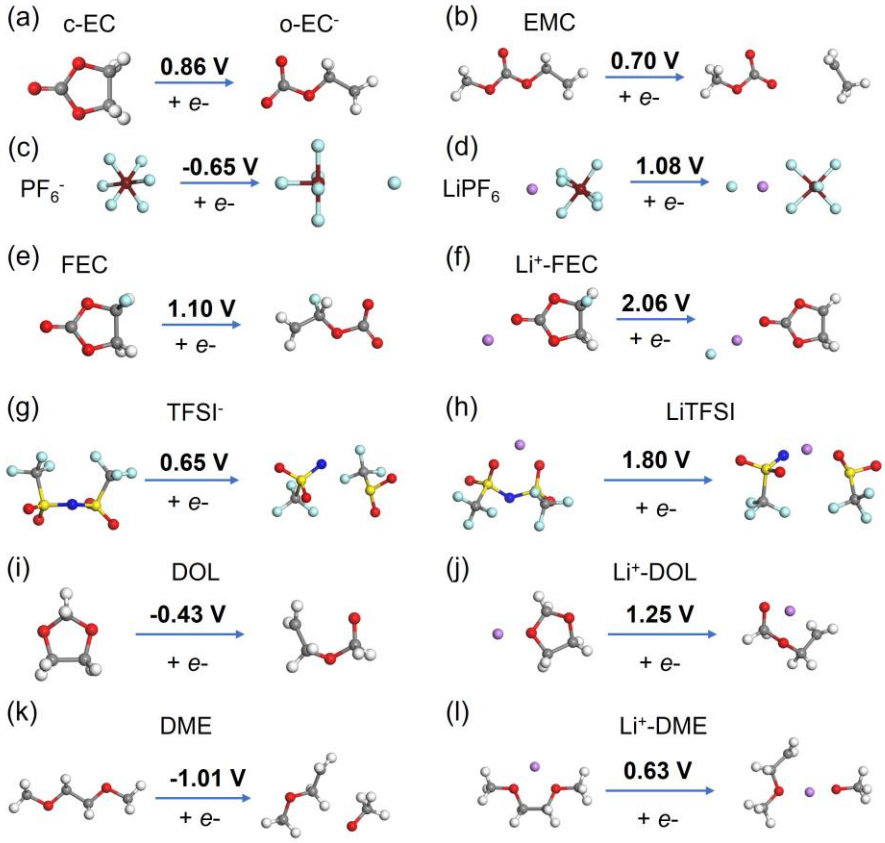

Figure S10. DFT-optimized geometries of the redox species and calculated reduction potentials for: (a) cyclic EC (c-EC), (b) EMC, (c) PF_6^-, (d) $LiPF_6$, (e) FEC and (f) Li^+-FEC, (g) $TFSI^-$, (h) LiTFSI, (i) DOL, (j) Li^+-DOL, (k) DME, and (f) Li^+-DME. The gray, red, white, purple, brown, and light blue, yellow, and dark blue spheres stand for C, O, H, Li, P, F, S and N atoms, respectively. Note that different decomposition mechanisms may have varied reduction potentials, as have been extensively investigated in the literature.[6–9] Here we only report the decomposition with the highest reduction potentials for clarity.

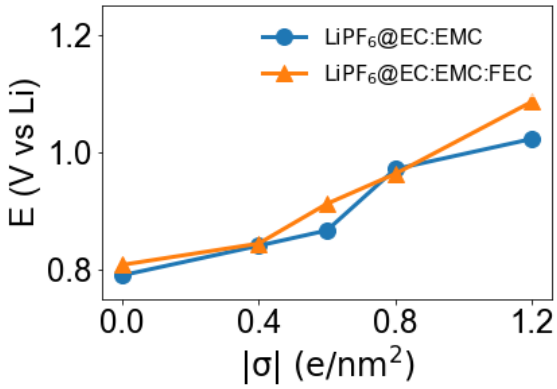

Figure S11. Averaged reduction potentials of the electrolyte species in the EDL as functions of the graphene electrode charge densities for the $LiPF_6$@EC:EMC and $LiPF_6$@EC:EMC:FEC electrolytes.

Part V, EDL structures of ether-based electrolytes

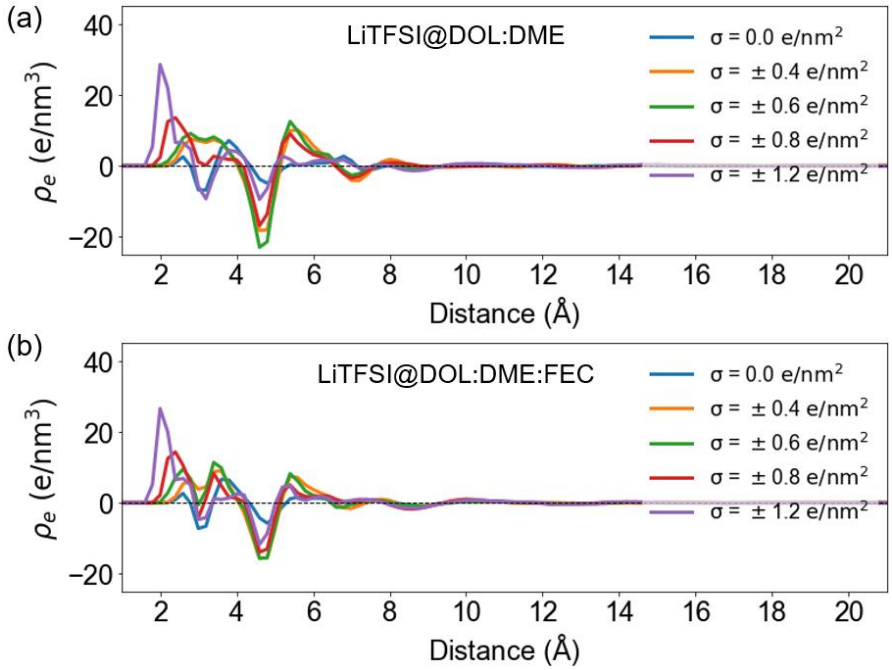

Figure S12. Charge density profiles for (a) LiTFSI@DOL:DME and (b) LiTFSI@DOL:DME:FEC electrolytes simulated at 20 ℃.

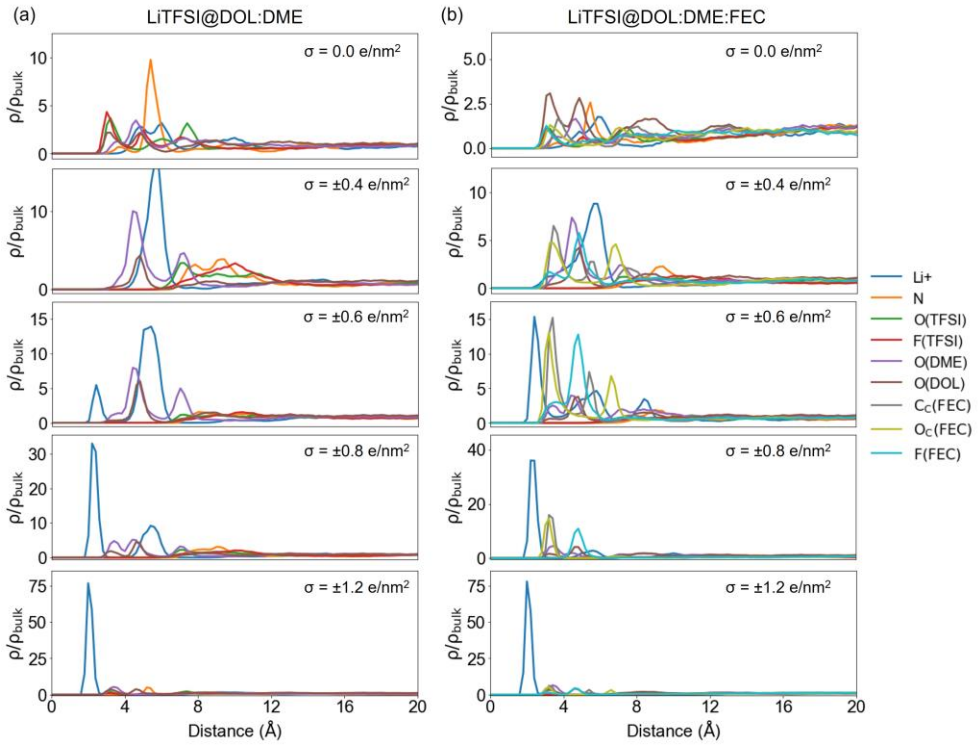

Figure S13. Normalized number density profiles of Li^+ ions and the atoms of interest in $TFSI^-$, DOL, DME, and FEC for (a) LiTFSI@DOL:DME and (b) LiTFSI@DOL:DME:FEC at 20 ℃ under different charge densities for the graphene electrode.

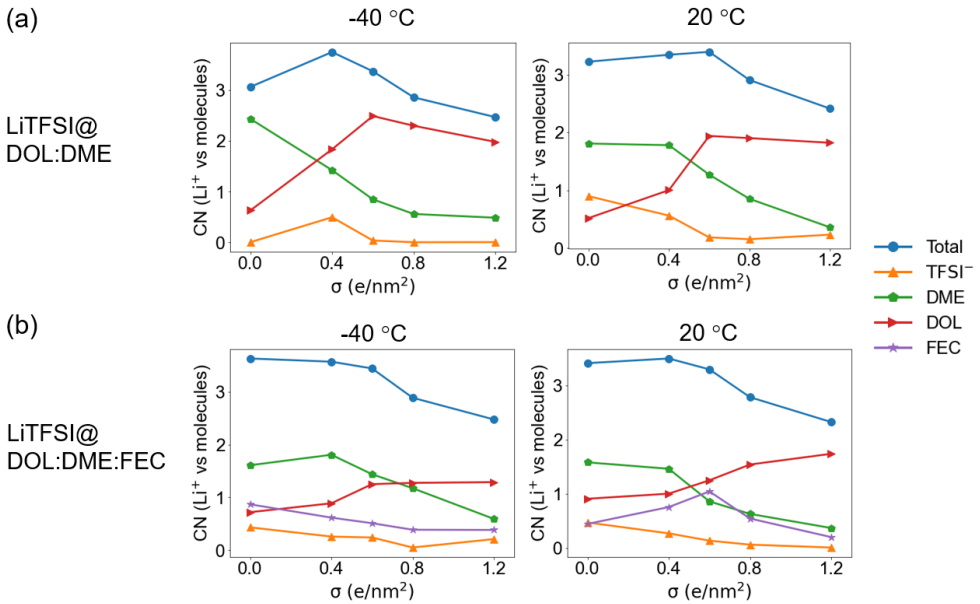

Figure S14. Coordination numbers between the Li^+ ions within the EDL and other molecular species ($TFSI^-$, DOL, DME and FEC) as functions of graphene electrode charge density at different temperatures (-40 ℃ and 20 ℃) for (a) LiTFSI@DOL:DME and (b) LiTFSI@DOL:DME:FEC electrolytes.

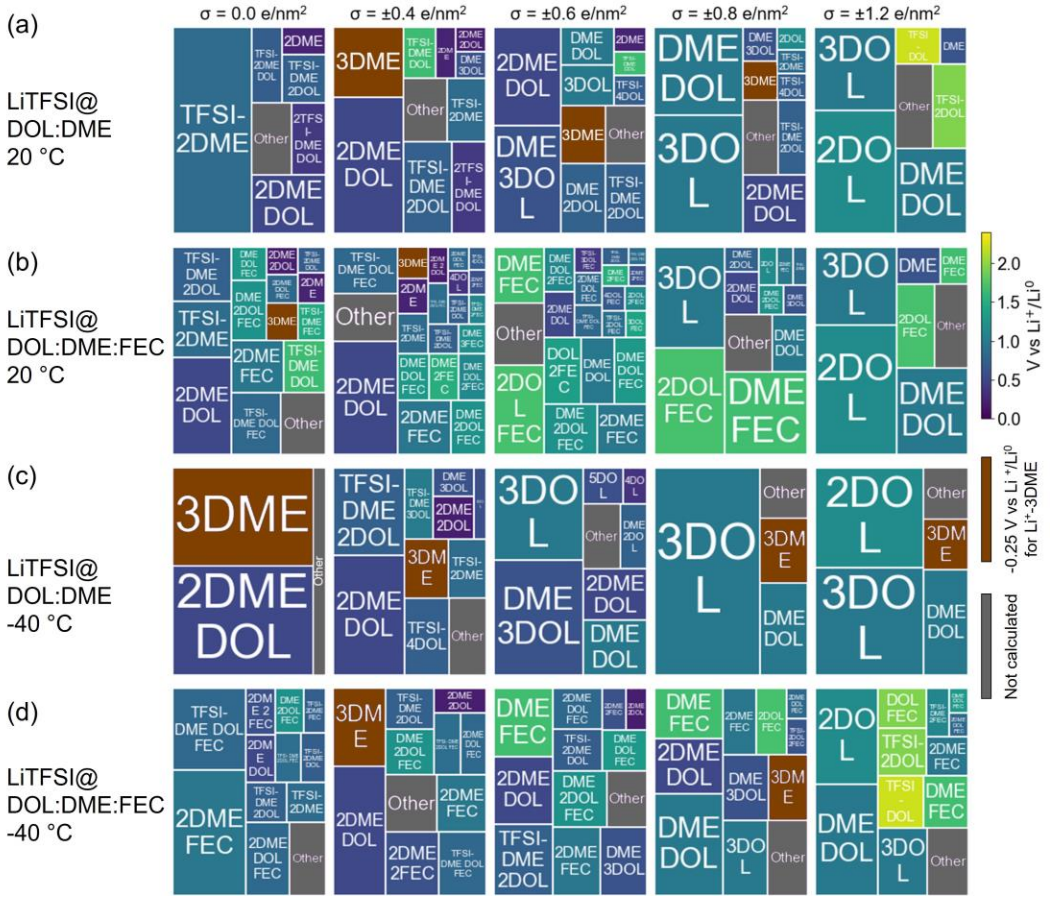

Figure 15. Probability distributions of the solvation structures of the first solvation shell of Li^+ ions within the EDL (10.0 Å from the negatively charged graphene electrode) under different graphene electrode charge densities (σ = 0.0, ±0.4, ±0.6, ±0.8 and ±1.2 e/nm^2) for (a) LiTFSI@DOL:DME electrolyte at 20 ℃, (b) LiTFSI@DOL:DME:FEC electrolyte at 20 ℃, (c) LiTFSI@DOL:DME electrolyte at -40 ℃ and (d) LiTFSI@DOL:DME:FEC electrolyte at -40 ℃. Those solvation shell structures with the highest probabilities that accumulate up to 90% are shown with their reduction potentials (indicated by color coding), while the rest is labeled with "Other" (in gray). All Li^+-coordinated clusters have positive reduction potentials *vs* Li^+/Li^0 except for Li^+-3DME, which has a negative potential of -0.25 V *vs* Li^+/Li^0 as denoted in brown.

References:

[1] Lee, J. Z.; Wynn, T. A.; Schroeder, M. A.; Alvarado, J.; Wang, X.; Xu, K.; Meng, Y. S. Cryogenic Focused Ion Beam Characterization of Lithium Metal Anodes. *ACS Energy Lett.* **2019**, *4* (2), 489–493.

[2] Saunier, J.; Gorecki, W.; Alloin, F.; Sanchez, J. Y. NMR Study of Cation, Anion, and Solvent Mobilities in Macroporous Poly(Vinylidene Fluoride). *J. Phys. Chem. B* **2005**, *109* (7), 2487–2492.

[3] Borodin, O.; Smith, G. D. Quantum Chemistry and Molecular Dynamics Simulation Study of Dimethyl Carbonate: Ethylene Carbonate Electrolytes Doped with LiPF6. *J. Phys. Chem. B* **2009**, *113* (6), 1763–1776.

[4] Thenuwara, A. C.; Shetty, P. P.; Kondekar, N.; Sandoval, S. E.; Cavallaro, K.; May, R.; Yang, C. T.; Marbella, L. E.; Qi, Y.; McDowell, M. T. Efficient Low-Temperature Cycling of Lithium Metal Anodes by Tailoring the Solid-Electrolyte Interphase. *ACS Energy Lett.* **2020**, *5* (7), 2411–2420.

[5] Thenuwara, A. C.; Shetty, P. P.; McDowell, M. T. Distinct Nanoscale Interphases and Morphology of Lithium Metal Electrodes Operating at Low Temperatures. *Nano Lett.* **2019**, *19* (12), 8664–8672.

[6] Borodin, O.; Olguin, M.; Spear, C. E.; Leiter, K. W.; Knap, J. Towards High Throughput Screening of Electrochemical Stability of Battery Electrolytes. *Nanotechnology* **2015**, *26* (35), 354003.

[7] Borodin, O.; Olguin, M.; Spear, C. E.; Leiter, K. W.; Knap, J.; Yushin, G.; Childs, A. S.; Xu, K. (Invited) Challenges with Quantum Chemistry-Based Screening of Electrochemical Stability of Lithium Battery Electrolytes. *ECS Trans.* **2015**, *69* (1), 113–123.

[8] Borodin, O.; Ren, X.; Vatamanu, J.; Von Wald Cresce, A.; Knap, J.; Xu, K. Modeling Insight into Battery Electrolyte Electrochemical Stability and Interfacial Structure. *Acc. Chem. Res.* **2017**, *50* (12), 2886–2894.

[9] Camacho-Forero, L. E.; Balbuena, P. B. Effects of Charged Interfaces on Electrolyte Decomposition at the Lithium Metal Anode. *J. Power Sources* **2020**, *472* (March), 228449.